CrossMark

Time reversal acoustics applied to rooms of various reverberation times

Michael H. Denison and Brian E. Anderson[a)]
Acoustics Research Group, Department of Physics and Astronomy, Brigham Young University, N283 Eyring Science Center, Provo, Utah 84602, USA

(Received 21 July 2018; revised 6 November 2018; accepted 8 November 2018; published online 3 December 2018)

Time Reversal (TR) is a technique that may be used to focus an acoustic signal at a particular point in space. While many variables contribute to the quality of TR focusing of sound in a particular room, the most important have been shown to be the number of sound sources, signal bandwidth, and absorption properties of the medium as noted by Ribay, de Rosny, and Fink [J. Acoust. Soc. Am. **117**(5), 2866–2872 (2005)]. However, the effect of room size on TR focusing has not been explored. Using the image source method algorithm proposed by Allen and Berkley [J. Acoust. Soc. Am. **65**(4), 943–950 (1979)], TR focusing was simulated in a variety of rooms with different absorption and volume properties. Experiments are also conducted in a couple rooms to verify the simulations. The peak focal amplitude, the temporal focus quality, and the spatial focus clarity are defined and calculated for each simulation. The results are used to determine the effects of absorption and room volume on TR. Less absorption increases the amplitude of the focusing and spatial clarity while decreasing temporal quality. Dissimilarly, larger volumes decrease focal amplitude and spatial clarity while increasing temporal quality. © *2018 Acoustical Society of America*.
https://doi.org/10.1121/1.5080560

[EF-G] Pages: 3055–3066

I. INTRODUCTION

Originally developed for acoustic signal transmissions in the ocean,[1,2] time reversal (TR) is a process used for focusing wave energy at a particular point in space.[3,4] TR has been used in a variety of acoustics applications, including high-energy focusing for ultrasound medical operations (i.e., lithotripsy),[5] the reconstruction of source events (i.e., earthquakes),[6] communications in reverberant environments,[7–9] and performing nondestructive evaluations of materials.[10,11]

There are two steps to the TR process: the forward propagation and the backward propagation. First, an impulse response (or transfer function in the frequency domain) is obtained between a source and a receiver. Second, the impulse response, $h(t)$, is reversed in time to create the time reversed impulse response, $h(-t)$, which is then broadcast from the source. The response at the receiver is the convolution of $h(t)$ and $h(-t)$ [which is equivalent to the autocorrelation of $h(t)$[12]] and is known as the focal signal. The peak amplitude of the focal signal is the result of coherent addition of the direct sound between the source and receiver and the reverberant sound arrivals caused by the enclosure. Optimizing the TR process for sound focusing in rooms has been a recent area of research. Some applications require a high amplitude focus, while others require a very narrow and impulsive-like focus. TR in rooms is a fairly new field with a limited amount of published studies. A brief literature review containing key studies of TR in rooms is included below.

Candy *et al.*[7,13] and Meyer *et al.*[14] studied the feasibility of using TR for an acoustic point-to-point communication experiment in a highly reverberant room. They found that TR can be used to recover a transmitted information sequence with zero-symbol error. They improved communication quality through the reverberant medium by applying a linear equalization filter, an array of multiple sources, and other signal processing. They did not address how different room conditions might affect TR.

Yon *et al.*[15] performed an experimental study in a reverberation chamber and found that TR provides better temporal and spatial focusing than classical time-delay beamforming because it utilizes the multiple sound paths between the sound sources and focus location. They also found that increasing the number of sound sources and increasing the bandwidth of the impulse response decreases the spatial side lobe level, which results in improved TR focusing. They concluded that side lobe levels are lower in a reverberant room than a free field but did not define any relationship between reverberation time and TR focusing performance. In their study, a 20-loudspeaker linear array was used to transmit the TR signal, and a single microphone on a one-dimensional scanning system was used to measure the temporal and spatial focus response. They defined a side lobe level as the difference in level between the focal point and the closest measureable side lobe in space.

Ribay *et al.*[16] used a time-domain, finite-difference numerical simulation that was used in previous TR studies in solids[17,18] and related them to room acoustics. They asserted that the peak focal amplitude is $N\tau/\tau_0$, where N is the number of TR transceivers, τ is the reverberation time of the room, and τ_0 is the width of the peak of the focused signal, based on the work of Draeger *et al.*[17,19] Thus, any change to the reverberation time should lead to a linear change in peak

a)Electronic mail: bea@byu.edu

amplitude of the focused signal. This relationship is stated but not explicitly shown, numerically or experimentally, neither in their paper nor in the papers cited.

Anderson *et al.*[20] explored the effect that source directivity has on TR in a room. They found that pointing the loudspeaker source away from the focus location increased the amount of energy in the reverberant field and led to a stronger focal signal amplitude in a highly reverberant room (reverberation time of 6.89 s). However, pointing the source towards the focus location led to a more impulsive like focus (higher temporal focus quality) and a more locally isolated focus (higher spatial focus clarity). In a less reverberant room, with $RT_{60} = 0.65\,s$, the direction of the source did not greatly affect the peak focal amplitude. Thus, the reverberation time of the room, the directivity of the source, and direction the source is facing has a dramatic effect on the TR process.

Willardson *et al.*[21] explored the application of TR to produce high amplitude focusing in a reverberant environment. They investigated how TR focusing changed depending on different signal processing strategies applied to $h(-t)$ prior to the backward step of the TR process. When comparing deconvolution, one-bit, clipping, and decay compensation signal processing strategies, they found that clipping produced the highest amplitude focal signal. The experiments were done in a reverberation chamber and did not explore the effects of these processing techniques in different rooms.

The purpose of this paper is to closely study the effects of wall absorption and room volume on the TR process, which is not fully shown in the literature. Numerical simulations and experimental results are used to show that the relationship between peak focal amplitude and reverberation time given by Ribay *et al.*[16] is true only when reverberation time is changed by modifying the absorption of the walls in the room. A new relationship between peak focal amplitude and reverberation time is shown when the reverberation time changes due to changing volume and the absorption is unchanged. Additionally, the temporal quality metric (how well TR focuses sound in time) and a new spatial clarity metric (a new metric that describes how well TR focuses sound in space) are defined and explored for multiple room enclosures. Testing the effects that absorption and room volume have on TR requires many room configurations. Simulations are used to determine the impacts of absorption and room volume on TR focusing due to the practical challenges of performing TR experimentally in many different rooms. However, experimental data are taken in a couple rooms to partly validate the simulated results. Reciprocal TR is used throughout the simulations and experiments.[4]

The image source method is used for the simulations in this study. The method assumes a rectangular parallelepiped room, uniform absorption on all of the walls, frequency-independent absorption (except in Sec. III C), omnidirectional and frequency-independent sources and receivers, specular reflections only, and no scattering from objects in the room. Although the inclusion of scattering surfaces has been shown to improve TR focusing,[3] scattering is excluded from the simulations to improve computational efficiency.

II. NUMERIC ACOUSTIC SIMULATION AND TR METRICS

An adequate numerical acoustic simulation for this study must be able to compute an impulse response, $h_{AB}(t)$, between a source at location A and a receiver at location B within a room enclosure. In the TR process, assuming a frequency-independent source, $h_{AB}(-t)$ is then convolved with $h_{AB}(t)$ to form the focal signal, $f(t)$

$$f(t) = h_{AB}(-t) * h_{AB}(t) = \int_{-\infty}^{\infty} h_{AB}(-\tau)h_{AB}(t-\tau)d\tau, \\ = R_{h_{AB}h_{AB}}(-t) = R_{h_{AB}h_{AB}}(t). \quad (1)$$

In Eq. (1), the $*$ denotes a convolution, τ is an integration dummy variable, and $R_{hh}(t)$ is the autocorrelation of $h(t)$, defined as[22]

$$R_{hh}(t) = \int_{-\infty}^{\infty} h(\tau)h(t+\tau)d\tau. \quad (2)$$

Because the autocorrelation function is a real and even function, $R_{h_{AB}h_{AB}}(t) = R_{h_{AB}h_{AB}}(-t)$. Thus, the focal signal is simply the autocorrelation of $h_{AB}(t)$.[7,12]

To simulate the response at an away location, C, during the backward propagation due to TR focusing at the focus location, B, an away location impulse response, $h_{AC}(t)$, is computed. The response at the away location, $a(t)$, is the convolution between $h_{AB}(-t)$ and $h_{AC}(t)$

$$a(t) = h_{AB}(-t) * h_{AC}(t) \\ = \int_{-\infty}^{\infty} h_{AB}(-\tau)h_{AC}(t-\tau)d\tau = R_{h_{AB}h_{AC}}(-t). \quad (3)$$

Thus, the response at an away location, C, is the time-reversed, cross correlation of $h_{AB}(t)$ and $h_{AC}(t)$. Because cross correlations and autocorrelations are much more computationally efficient than convolutions, this paper simulates $f(t)$ by computing the autocorrelation of $h_{AB}(t)$ and $a(t)$ by computing the time-reversed, cross correlation of h_{AB} and h_{AC}.

When experimentally performing TR, it is common practice to normalize $h_{AB}(-t)$ to the peak input voltage of the amplifier before broadcasting it from the sound source in order to maximize the focal amplitude. Similarly, each simulated $h_{AB}(-t)$ is normalized to have a peak amplitude of one before convolving it with $h_{AB}(t)$. Thus, the autocorrelation and cross correlation results are scaled by the appropriate normalization factor to set the peak amplitude of $h_{AB}(-t)$ to one.

A. Image source method

The image source method models specular reflections off of room surfaces as sound coming from image sources outside of the room. In a closed room, every surface acts as a mirror that creates an image source.[23] For a rectangular parallelepiped room, the parallel surfaces create image rooms that expand out in three dimensions (including diagonal directions), with each having its own image source. Each image source contributes to a specific part of the simulated $h(t)$. During a simulation, all real and image sources simultaneously produce a ray of sound

that travels in a straight line between itself and the receiver. The ray loses amplitude according to spherical spreading as it travels. Additionally, every time a ray passes through a wall surface, the ray loses energy according to the wall surface's absorption coefficient. The time at which a ray reaches the receiver is determined by the speed of sound in traveling the distance between the receiver and a given image source. $h(t)$ is created by linearly superposing the contributions from each ray with the appropriate time delay. Figure 1 shows a two-dimensional representation of the image source method with only a few image sources.

The ray tracing method was also considered for this study. This method models sound as following multiple rays that expand in different directions from a source. The rays interact with the room by reflecting off surfaces, with some models including scattering instead of just specular reflections, and some of the sound energy being absorbed according to the absorption characteristics of each surface. Every ray that passes through the defined receiver region is recorded along with the relative amplitude and time of arrival of the sound waves associated with each ray. Finally, the signals are added together to form an impulse response. Ray tracing methods can model the inclusion of irregular room geometries and scattering objects (e.g., tables and chairs). Ray tracing normally requires millions of rays or more for accuracy. Depending on the room size, number of rays used, and the available computational power, a single impulse response may take several hours to calculate. The results presented in this paper required simulations conducted in many different rooms, corresponding to thousands of impulse responses; thus, the inefficiencies associated with ray tracing made it an impractical approach. Additionally, the defined receiver region would limit spatial precision and may affect the exact time of arrival of each ray, whose timing is of critical importance in the TR process. The image source method only uses the exact number of rays that reach the microphone within a desired time interval and, thus, it is more computationally efficient.

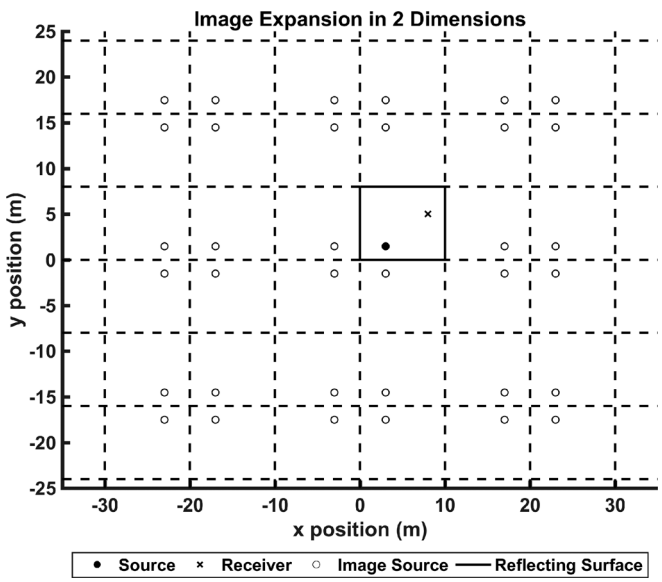

FIG. 1. A two-dimensional representation of the image source method. The solid lines represent the original room, while dotted lines represent image rooms. The figure is limited to only a few image sources for simplicity. The actual image space is three-dimensional and includes many more image sources.

The Allen and Berkley Image Source Method is an efficient and simple algorithm that can be easily implemented in many computational programs.[24] It is a relatively simple approach to modeling room acoustics and thus possesses certain limitations. The model assumes a rectangular parallelepiped room and, therefore, cannot be used for rooms with complicated geometries. The model also assumes that the room is empty, meaning that it does not account for scattering and absorption of sound from objects in the room. The model assumes an omnidirectional source and receiver, each possessing an idealized flat frequency response. Finally, each of the six surfaces in the room must have uniform, frequency-independent absorption coefficients, meaning that it cannot account for irregular absorption regions on a given wall (like an open window or absorptive panel), and the model is restricted to specular wall reflections (i.e., scattering coefficients of walls are not included). A high pass filter at 500 Hz is used to eliminate nonphysical effects near zero frequency and to stay above a typical Schroeder frequency value for the rooms. Although this approach limits a TR study to simple rooms, it is advantageous over other modeling methods because of its computational efficiency and because there is no need to export data from commercial software packages to simulate TR focusing. Figure 2 shows an example of a one-second impulse response created with this method, $h_{AB}(t)$, and the corresponding focal signal, $f(t)$, and a response away from the focus location, $a(t)$.

The peak energy of the focal signal is located at the center of the focal signal, as seen in Fig. 2(b). The side lobes or "noise" appearing before and after the peak energy of the focal signal are a consequence of the autocorrelation and are physically caused by transducers being unable to retrace only the original direct and reverberant sound paths.

Additional work has been done to further improve the original Allen and Berkley Image Source Method. Peterson[25] found that applying a low-pass filter to the impulse response improves arrival time accuracy. A similar approach is followed in this paper by band limiting impulse responses between 500 and 7500 Hz. The upper frequency limit of 7500 Hz was chosen based on the results from Willardson *et al.*,[21] who found that including frequencies above 7500 Hz did not greatly impact TR focusing. Additionally, incorporating phase shifts at each sound reflection leads to a better approximation of an impulse response.[26] Unfortunately, incorporating these phase shifts led to much higher computation time, thus this modification was not incorporated in this study.

B. Temporal focus quality

Many applications of TR require that the focal signals have a narrow temporal envelope. In communications applications, the focal signal is the carrier signal for the intended message. The resulting signal at the focus location is the convolution of the focal signal and the intended message.

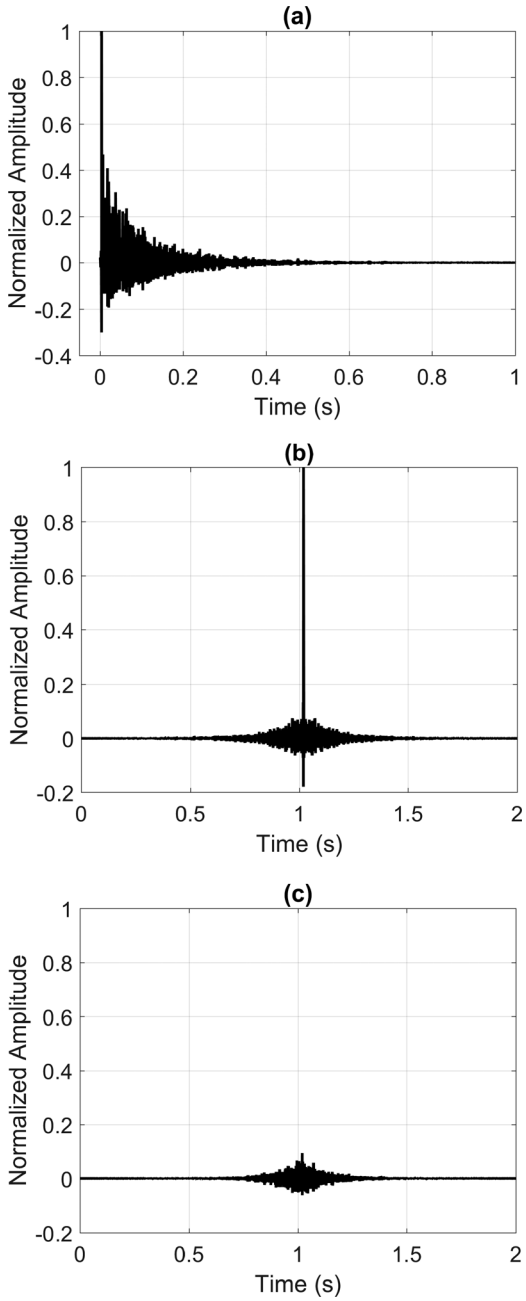

FIG. 2. (a) An example of a normalized impulse response generated by the Allen and Berkley Image Source Method. (b) The corresponding normalized focal signal, $f(t)$. (c) A response away from the focus location normalized by the same value as the focal signal, $a(t)$.

The ideal, but practically impossible focal signal would be a delta function. This would result in a perfect transmission of the message. The side lobes before and after the peak amplitude of the focal signal [Fig. 2(b)] and the band limited nature of transducers result in asynchronous repetitions of the intended message at the focus location.

Temporal focus quality is a metric that describes how well a focal signal approximates a delta function. It compares the peak focal amplitude, f_P, with the total energy of the focal signal $f(t)$. While different definitions of temporal quality have been used in the past,[18,21,27,28] this paper uses a modified version of the metric defined by Heaton *et al.*[28]

$$\xi_T = \sqrt{\frac{[f_P]^2}{\frac{1}{M}\sum_{m=1}^{M}\left[f(x_0, y_0, z_0, m)\right]^2}}, \tag{4}$$

where $f(x_0, y_0, z_0, m)$ is the amplitude of the of the mth sample of the focal signal at the focal position (x_0, y_0, z_0) and M is the number of discrete samples in the signal. ξ_T is a unitless metric that, in the case of room acoustics, is effectively the ratio of peak pressure amplitude to the average pressure amplitude of the entire signal. ξ_T is also equivalent to what Derode *et al.*[18] called the signal-to-noise ratio (SNR), which is defined as the peak amplitude divided by the standard deviation of the surrounding noise (not including the peak amplitude), σ, or $SNR = f_P/\sigma$. Additionally, ξ_T is nearly identical to the so called contrast metric, which is the ratio of the intensity of f_P to the intensity in the rest of the signal (again the f_P intensity is not included).[29] Finally, one more difference between ξ_T and the SNR defined by Derode *et al.*[18] is that ξ_T depends on the length of the signal while the SNR from Derode *et al.* does not; $\xi_T \approx M$ and the SNR from Derode *et al.* $\approx\infty$ as the focal signal approaches a delta function.

As an example, the maximum temporal quality possible occurs when the signal is a delta function, which results in $\xi_T = \sqrt{M}$. As seen in Fig. 2(b), most focal signals approach zero amplitude at the start and end of the time window. Consequently, ξ_T can be arbitrarily increased or decreased by measuring more or less samples in the recording. Therefore, ξ_T is best used as a relative measure of temporal quality of various signals of the same length rather than as an absolute measure of temporal quality.

Equation (4) is typically used to calculate ξ_T for the focal signal but it can be used to calculate ξ_T for the response at any location. This is done by generalizing $f(x_0, y_0, z_0, m)$ with $g(x, y, z, m)$, the signal recorded at position (x, y, z) during the focusing. f_P is changed to g_P, the peak amplitude of $g(x, y, z, m)$. ξ_T for the focal signal shown in Fig. 2(b) is 94.2, while the away signal shown in Fig. 2(c) has a value of 17.1. The higher value of ξ_T for the focused signal is due to a much larger peak amplitude.

C. Spatial focus clarity

Many applications of TR also require that strong temporal focusing only occurs at a single location. For example, in communications applications, it is important that the delivered message is only focused at the intended location and not able to be intercepted at other locations. Spatial focusing metrics have been developed by others to describe the ratio of f_P at the focus location to the amplitudes at other spatial locations.[20,27] Heaton *et al.*[28] also provided a metric for the TR spatial focus quality, ξ_S, that relates the peak amplitude at the focus location to the amplitude of other locations at the time of peak focusing. Similarly, Yon *et al.*[15] quantifies spatial focusing using side lobe level, which is the ratio of f_P and the largest spatial side lobe amplitude over time.

The spatial focus clarity, Λ_S, is a new metric and is the ratio of temporal quality at the focus point to the average

temporal quality over all spatial positions in a two-dimensional region of interest (ROI), and is thus a spatial measure of ξ_T. This metric gives greater insight into the impulsive nature of the temporal signal at the focus location compared to the resulting signals elsewhere. For communication applications of TR, Λ_S can be used to determine the likelihood that the communication might be interpretable elsewhere in the ROI. This paper only considers two-dimensional ROIs along the x–y plane. TR spatial focus clarity is defined as

$$\Lambda_S = \sqrt{\frac{\left[\xi_T(x_0, y_0, z_0)\right]^2}{\frac{1}{N_x N_y}\sum_{n_x=1}^{N_x}\sum_{n_y=1}^{N_y}\left[\xi_T(n_x, n_y, z_0)\right]^2}}, \tag{5}$$

where (x_0, y_0, z_0) is the Cartesian coordinates for the focus location, N_x and N_y are the number of measurement locations in the x and y directions, respectively, in the ROI, and $\xi_T(n_x, n_y, z_0)$ is the temporal quality at the (n_x, n_y, z_0) location within the ROI. Λ_S can be made to represent three dimensions by replacing $\xi_T(n_x, n_y, z_0)$ with $\xi_T(n_x, n_y, n_z)$, multiplying by $1/N_z$ in the denominator and including a third summation over n_z up to N_z. Additionally, Λ_S can be evaluated for two-dimensional ROIs along planes other than the x–y plane by substituting N_x, N_y, n_x, and n_y with the appropriate plane variables. Similar to ξ_T, the value of Λ_S can change greatly depending on the values of N_x and N_y and is thus a relative measure of the quality of spatial focusing. Therefore, when comparing multiple TR experiments with different ROIs, each should have the same values for N_x and N_y and grid spacing. Λ_S equals one for anechoic and direct sound exclusive fields because values of ξ_T will be equal at all points in the ROI.

Calculating Λ_S requires the response at every grid location in a ROI due to the source broadcasting $h_{AB}(-t)$. To do this, impulse responses are simulated between the source location and each location, $h_{AC}(t)$, within a ROI and the response is then calculated by computing the time reversed cross correlation between $h_{AB}(t)$ and $h_{AC}(t)$. Figure 3 shows the room dimensions along with source, focus, and ROI locations for the example simulation. The room shown is an $8.8 \times 11.1 \times 7$ m rectangular room and the average absorption coefficient of the room is 0.04. The source is located at $(7, 6, 3)$ m and the focus is at $(4, 6, 3)$ m with a one-meter ROI around the focus with 2 mm grid spacing for a total of 251 001 ROI grid points, each requiring a unique impulse response. Figure 4(a) shows a spatial focus map in dB, which represents the instantaneous sound pressure level (SPL) response at locations within the ROI at the time of peak focus (normalized with respect to the SPL value for f_P). The focus location, $(0.5, 0.5)$ m, is shown to have the expected maximum response. A feature in Fig. 4(a) that spans along the y direction and near 4 meters in the x direction is shown to have higher than average response. This feature is a result of direct sound coming from the sound source located three meters away, (to the right as pictured) along the x direction, as seen in Fig. 4. The high amplitude feature at the focus location is caused by the coherent addition inherent in the TR process.

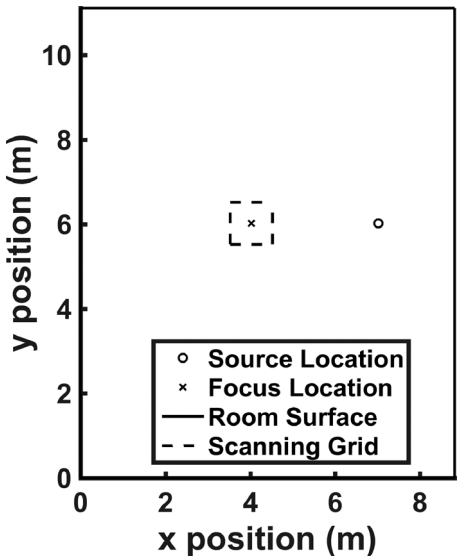

FIG. 3. Example room dimensions along with source, focus, and ROI scanning grid locations that were used to simulate the results of Fig. 4.

Figure 4(b) shows a map of $\xi_T(n_x, n_y)$, normalized with respect to $\xi_T(n_0, n_0)$, in dB. The figure shows how ξ_T is

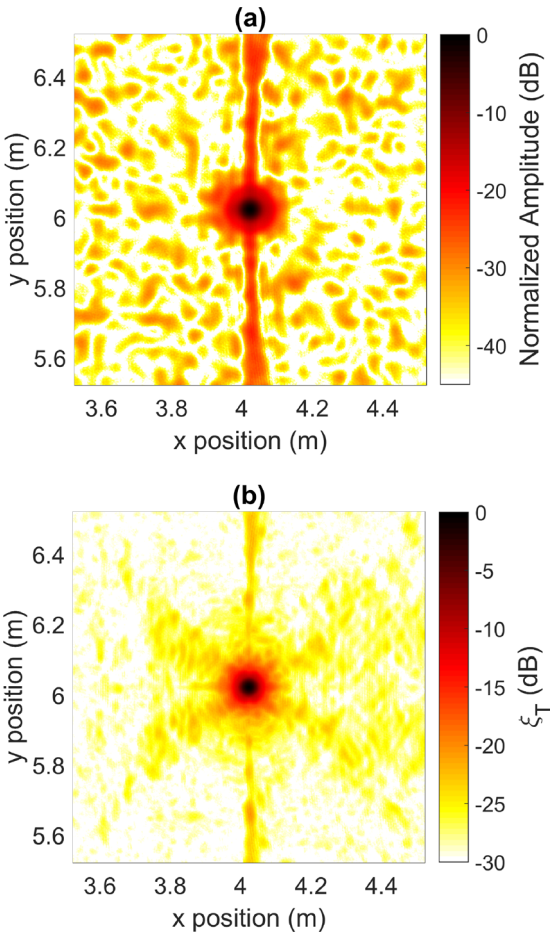

FIG. 4. (Color online) (a) Typical spatial distribution of simulated time reversal focusing in dB re peak. (b) Typical spatial distribution of the temporal focus quality, ξ_T, in dB re peak from normalized simulation results. Note that the sound source is located 3 meters along x to the right from the center of each map.

maximized at the focus location $(4, 6)$ m and how it relates to other locations on the surface, $\xi_T(n_x, n_y)$.

III. SIMULATED RESULTS

TR simulations were created to more easily determine the effects of wall sound absorption in a room and room volume on f_P, ξ_T, and Λ_S. The Allen and Berkley Image Source Method was implemented in MATLAB in order to simulate impulse responses. Additional filtering was included to limit the frequency range of the impulse responses from 500 to 7500 Hz, which closely resembles the experimental procedures outlined in Sec. IV and ensures that the frequencies used are above the Schroeder frequency.[30] Each impulse response was 0.8 s in length and sampled at 50 kHz. Impulse responses recorded longer than 0.8 s and used for time reversal focusing did not greatly affect the focal signal nor the responses obtained across the ROI. The values obtained for the metrics we use to evaluate time reversal focusing changed slightly when the impulse responses were longer than 0.8 s, but the trends were the same. The autocorrelation of $h(t)_{AB}$ was used to determine the focal signal. The focal signal was used to calculate f_P and ξ_T according to Eq. (4). As seen in Eq. (5), Λ_S requires individual values of ξ_T for each location on the ROI. The response at each location was simulated at each grid point in the 1×1 m ROI with 10 cm spacing resulting in 121 scanning points. Ten centimeter spacing was determined to be sufficient to accurately calculate Λ_S for this study, meaning that the trends (shown later on) for Λ_S did not change significantly for finer spacing. Finer spacing would be necessary to study other features of TR focusing, such as the spatial focal spot width. Λ_S is computed for each ROI and then the RT_{60} is changed (either by changing the absorption characteristics of the room or the volume of the room) and the simulation is conducted. Source, focus, and measurement grid locations were placed at least 1 m away from any surface to minimize boundary effects and ensure a diffuse field.[31]

A. Changing absorption

In order to minimize the likelihood of degenerate modes, a room with an ideal aspect ratio[31] $2^{1/3} : 4^{1/3} : 1$ with dimensions $3.78 \times 4.76 \times 3.00$ meters and with a uniform absorption coefficient of 0.18 on all six surfaces was used to create the initial simulated room. This room had a predicted RT_{60} of 0.5 s using the Norris-Eyring reverberation formula[32,33]

$$RT_{60} = -\frac{24(\ln 10)V}{cS\ln\left(1 - \langle\alpha\rangle_S\right)}, \tag{6}$$

where V is the volume of the room, $\langle\alpha\rangle_S$ is the absorption coefficient averaged over the room surface area, and S is the surface area of the room, and the factor of 0.161 assumes metric units (meters, kilograms, seconds, MKS system) and a speed of sound of 343 m/s. To isolate the effect that absorption has on TR, $\langle\alpha\rangle_S$ was systematically lowered (from 0.18 to 0.03) to create 26 simulated rooms such that RT_{60} spans from 0.5 to 3.0 s with 0.1 s increments. Note that the exponential decay times [i.e., Norris-Eyring absorption times, τ_{NE}, where the sound pressure is assumed to decay at a rate of $e^{-t/(2\tau_{NE})}$, where $\tau_{NE} = -4V/\ cS\ln(1 - \langle\alpha\rangle_S)]$ for the rooms modeled range from 36 ms for the 0.5 s RT_{60} room, in a linear fashion, up to 217 ms for the 3.0 s RT_{60} room. Also, the Heisenberg time (defined as $t_H = 2\pi n$,[34,35] where n is the modal density, is equivalent to the inverse of the mean spacing between modal frequencies) for the lowest frequency employed (500 Hz) for all rooms was 30 s. Finally, the Schroeder frequencies[30] [defined as $f_S = \sqrt{(c^3/4\ln 10)(RT_{60}/V)}$] ranged from 201 Hz for the 0.5 s RT_{60} room up to 493 Hz for the 3.0 s RT_{60} room. Because $\tau_{NE} \ll t_H$ and the frequencies employed are $f > f_S$, the sound field in these rooms is considered to be diffuse where ray tracing is entirely appropriate, although the ray propagation may not qualify as being ergodic due to the parallelepiped room geometries. Further, the 0.8 s recording length of the impulse response is always longer than the absorption time for each room and always much less than t_H.

The source location is (2.34, 2.01, 1.01) m and the focus location is (1.50, 2.85, 1.01) m. For each of the room conditions, f_P, ξ_T, and Λ_S were calculated using the method described previously. Relationships between the Norris-Eyring RT_{60} and f_P, ξ_T, and Λ_S for the 26 rooms are shown by the solid lines of Fig. 5. For f_P, increasing RT_{60} by decreasing $\langle\alpha\rangle_S$ leads to a linear relationship between f_P and RT_{60} (coefficient of determination, $R^2 = 0.9997$). This follows the linear relation prediction from Ribay *et al.*[16] Decreasing $\langle\alpha\rangle_S$ also results in a slight lowering of ξ_T and a drastic increase in Λ_S. As RT_{60} changes from 0.5 s to 3 s, f_P increases by 515%, ξ_T decreases by only 2.4% and Λ_S increases by 264%, thus the increases in f_P and Λ_S are much more significant than the decrease in ξ_T. These trends are due to the increased amount of reverberant energy at the focus location as $\langle\alpha\rangle_S$ decreases. For Λ_S, increasing reverberant energy creates a less coherent sound field across the ROI, which decreases ξ_T at locations other than the focus. Though not presented here, the same trends were observed when simulating rooms with different initial volumes and varying the absorption.

According to Quieffin *et al.*[29] and Bou Matar *et al.*,[36] when $\tau_{NE} < t_H$ and τ_{NE} is less than the length of the impulse response used for time reversal, which is the case for all of the work presented in this paper, the contrast (which is similar to ξ_T but not the same) is proportional to τ_{NE}, which does not appear to be confirmed by the ξ_T results in Fig. 5 since τ_{NE} increases with increasing RT_{60}. However, the contrast metric does not include f_P in the calculation of the "noise," whereas it is included in the calculation of the noise in the ξ_T. Since f_P is shown in Fig. 5 to increase with RT_{60}, it is found that if f_P was not included in the calculation of the "noise" for ξ_T (making this metric identical to the contrast), then ξ_T does increase linearly as expected for the contrast, confirming the assertions of Quieffin *et al.*[29]

B. Changing volume

The same initial room, as used in Sec. III A, with dimensions $3.78 \times 4.76 \times 3.00$ m and with an average absorption coefficient of 0.18 was used to test the effect that changing

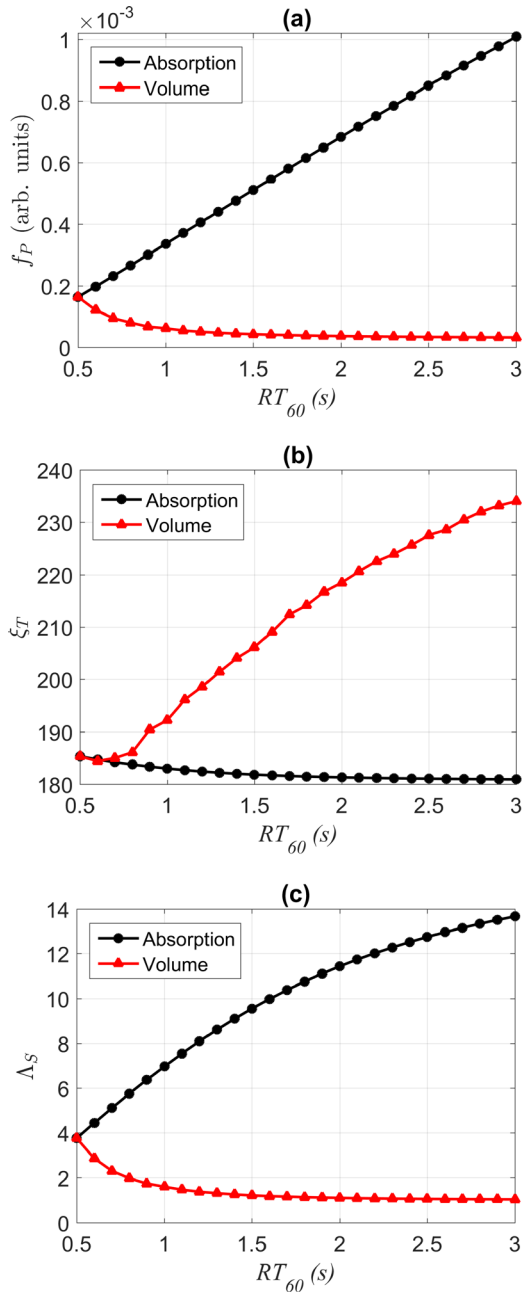

FIG. 5. (Color online) Simulation results for time reversal focusing metrics versus RT_{60} for various rooms of different frequency-independent absorption coefficients and room volumes. (a) Peak focal amplitude, f_p. (b) Temporal quality, ξ_T. (c) Spatial clarity, Λ_s.

volume has on TR. Using Eq. (6), $\langle\alpha\rangle_S$ was held constant and V was systematically increased to create 26 simulated rooms such that RT_{60} spans from 0.5 to 3 s with 0.1 s spacing. The aspect ratio $2^{1/3} : 4^{1/3} : 1$ was maintained for every simulated room in order to have a constant relationship between V and S. This resulted in V ranging in values from 54 m^3 for a $RT_{60} = 0.5$ s to 11 664 m^3 for a $RT_{60} = 3$ s. The exponential decay times for the rooms modeled range from 36 ms for the 0.5 s RT_{60} room up to 217 ms for the 3.0 s RT_{60} room. Also, the Heisenberg time for the lowest frequency employed (500 Hz) ranged from 30 s for the 0.5 s RT_{60} room up to 5800 s for the 3.0 s RT_{60} room. Finally, the Schroeder frequencies ranged from 201 Hz for the 0.5 s RT_{60} room down to 34 Hz for the 3.0 s RT_{60} room. Because $\tau_{NE} \ll t_H$ and the frequencies employed are $f > f_S$ the sound field in these rooms is considered diffuse. Again, the 0.8 s recording length of the impulse response is always longer than the absorption time for each room and always much less than t_H.

While the simulated rooms increased in size, the source and receiver/focus locations were held at a constant 1.18 m separation but were moved to be located near the geometric center of each room, which effectively resulted in the room expanding out in every direction around the source and focus locations. Figure 6 compares a plan view of the room configuration of the initial room with a volume of 54 m^3 and a room with a volume of 2963 m^3. For each of the room conditions, f_P, ξ_T, and Λ_S were calculated using the method described above. The dashed lines of Fig. 5 show the relationships between RT_{60} and f_P, ξ_T, and Λ_S.

Interestingly, increasing RT_{60} by increasing V leads to opposite trends compared to the changing absorption case. Increasing volume leads to lower f_P and Λ_S values and higher ξ_T values. f_P steadily decreases and approaches a minimum value corresponding to the direct sound from the source. Smaller rooms have many early reflections of high amplitude. For larger rooms, the first few reflections arrive later in time and have undergone more spherical spreading loss and thus contribute less to TR focusing. Similarly, Λ_S decreases and approaches a value of one for very large rooms. This is because for larger rooms, an ROI near the source becomes dominated more by the direct sound, which leads to a more uniform response across the ROI. Likewise, ξ_T increases for larger rooms because direct-sound dominated fields lead to more impulsive-like $h(t)$ and focal signals. As RT_{60} changes from 0.5 to 3 s due to changing volume, f_P decreases by 80%, ξ_T increases by 26%, and Λ_S decreases by 73%.

Contrary to the results of Ribay *et al.*,[16] the two distinct trends in Fig. 5(a) show that f_P is not always proportional to RT_{60}. For a given room of a fixed volume, changes in absorption follow the trend given by Ribay *et al.*,[16] but when the change in RT_{60} is due to volume changes, the trend not only breaks down, but there is an apparent opposite trend.

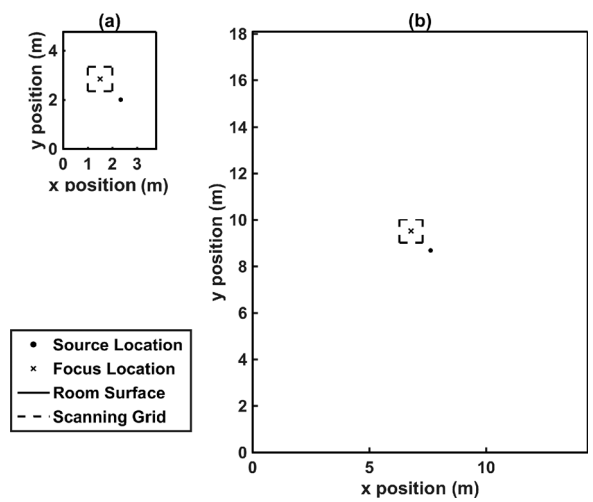

FIG. 6. Drawings of two simulated room configurations (a) with a volume of 54 m^3 and (b) with a volume of 2963 m^3.

This may be because the dependence given by Ribay *et al.*[16] was derived from work in solid media where the losses, aside from spherical spreading, are principally due to propagation absorption losses. In rooms, the losses are principally derived from reflections off of wall surfaces, and propagation losses are typically negligible in comparison.

Here, the ξ_T is shown to increase essentially linearly with RT_{60} and with τ_{NE} appearing to confirm the contract results of Quieffin *et al.*[29] However, if f_P were again excluded from the calculation of the noise in the ξ_T, then ξ_T decreases exponentially with RT_{60}. This is because f_P is shown in Fig. 5 to decrease exponentially with RT_{60}. Again, these results for the changing volume case differ from that expected according to the Quieffin *et al.*[29]

C. Frequency-dependent absorption

The original Allen and Berkley Image Source Method creates impulse responses using frequency-independent absorption coefficients.[24] In order to determine if frequency-dependent absorption characteristics of materials affect TR focusing, the image source method was modified to include frequency-dependent absorption coefficients specified at the octave-band center frequencies. This was done by performing the image source modeling with the absorption coefficient corresponding to a given octave band applied to every wall surface. A set of impulse responses for each location within the ROI is obtained. Octave band filtering, using an eighth-order, linear-phase, bandpass filter, is applied to the set of each impulse responses. This process is repeated for each octave-band absorption coefficient, and the impulse responses are filtered for that corresponding octave band of frequencies. After a set of impulse responses is obtained for each octave band, the band pass filtered signals are summed for each location to construct an impulse response with frequency-dependent absorption properties. It is this constructed set of impulse responses that is then used in the post-modeling simulations of TR. The constructed impulse response is then band limited from 500 to 7500 Hz to be consistent with the simulations in Secs. III A and III B.

The effects of changing absorption and volume on TR focusing were simulated using frequency-dependent absorption coefficients. Due to the difficulty of finding a wide variety of materials with different absorption characteristics that would lead to incremental changes in RT_{60}, a single material was chosen as a starting point and its frequency-dependent absorption coefficients were multiplicatively changed to produce a desired RT_{60}. Reverse Shroeder integration[37,38] was used to predict RT_{60} for each constructed impulse response with frequency-dependent absorption coefficients. In this study, gypsum board was chosen for its relatively low-frequency absorption coefficients. These low values permitted a wide range of absorption multipliers, allowing for high and low values for frequency-dependent absorption coefficients. Twenty-six multipliers were used, ranging from 0.25 to 8 with logarithmic spacing. Table I shows seven of the multipliers, the resulting frequency-dependent absorption coefficients ranging from 500 to 8000 Hz octave bands, and the resulting RT_{60} values. After including the frequency-dependent absorption, the constructed impulse response is band limited from 500 to 7500 Hz to match the simulations in Secs. III A and III B. A multiplier of one results in absorption coefficients equal to gypsum board.[39] The absorption coefficients of materials at 8000 Hz are not commonly measured, so the value of 0.110 at 8000 Hz was estimated.

TABLE I. Octave band frequency dependent absorption coefficients resulting from 7 of the 26 multipliers with the resulting RT_{60}.

	Absorption Coefficients					
Multiplier	500 Hz	1000 Hz	2000 Hz	4000 Hz	8000 Hz	RT_{60} (s)
0.250	0.013	0.010	0.018	0.023	0.028	3.61
0.287	0.014	0.011	0.020	0.026	0.032	3.39
….						
0.871	0.044	0.035	0.061	0.078	0.096	1.83
1.000	0.050	0.040	0.070	0.090	0.110	1.69
1.149	0.057	0.046	0.080	0.103	0.126	1.58
…						
6.964	0.348	0.279	0.488	0.627	0.766	0.25
8.000	0.400	0.320	0.560	0.720	0.880	0.22

In general, the results from simulations with frequency-dependent absorption shown in Fig. 7 are similar to the results with uniform frequency absorption. As before, decreasing absorption leads to higher f_P and Λ_S values and lower ξ_T values. f_P still follows a nearly linear trend with changing absorption (coefficient of determination, $R^2 = 0.9506$), although not as strictly linear as the frequency-independent absorption case. Like before, decreasing $\langle\alpha\rangle_S$ also results in a lowering of ξ_T and a drastic increase in Λ_S. Unique to the frequency-dependent absorption case is a minimum in ξ_T when $RT_{60} = 2$ s. From RT_{60} of 0.2 to 3.6 s, f_P increases by 3500%, ξ_T decreases by 16.5%, and Λ_S increases by 533%, thus the increases in f_P and Λ_S are again much more significant than the decrease in ξ_T. For the changing volume case, $\langle\alpha\rangle_S$ is held constant and set equal to the frequency-dependent absorption coefficients of gypsum board.[39] Like before, increasing volume leads to lower f_P and Λ_S values and higher ξ_T values. From a RT_{60} of 1.7 to 4.7 s, f_P decreases by 92%, ξ_T increases by 35% and Λ_S decreases by 419%.

In general, the inclusion of frequency dependent absorption in a room does not significantly impact the trends of how changing absorption and volume effect TR focusing. The key trends of increasing f_P and Λ_S and decreasing ξ_T when absorption or volume are decreased still hold.

IV. EXPERIMENTAL RESULTS

Experimental data was obtained in a few selected rooms in order to compare with the simulated results. This required two types of rooms: one with the ability to incrementally change the absorption while leaving the volume constant, and the other with the ability to change the volume while maintaining constant absorption.

In both experimental setups, a custom built 20 cm diameter dodecahedron loudspeaker, powered by a Crown CT4150 amplifier, was used as the sound source and a G.R.A.S. 46AQ 1.27 cm (0.5 in.) random-incidence microphone, powered by

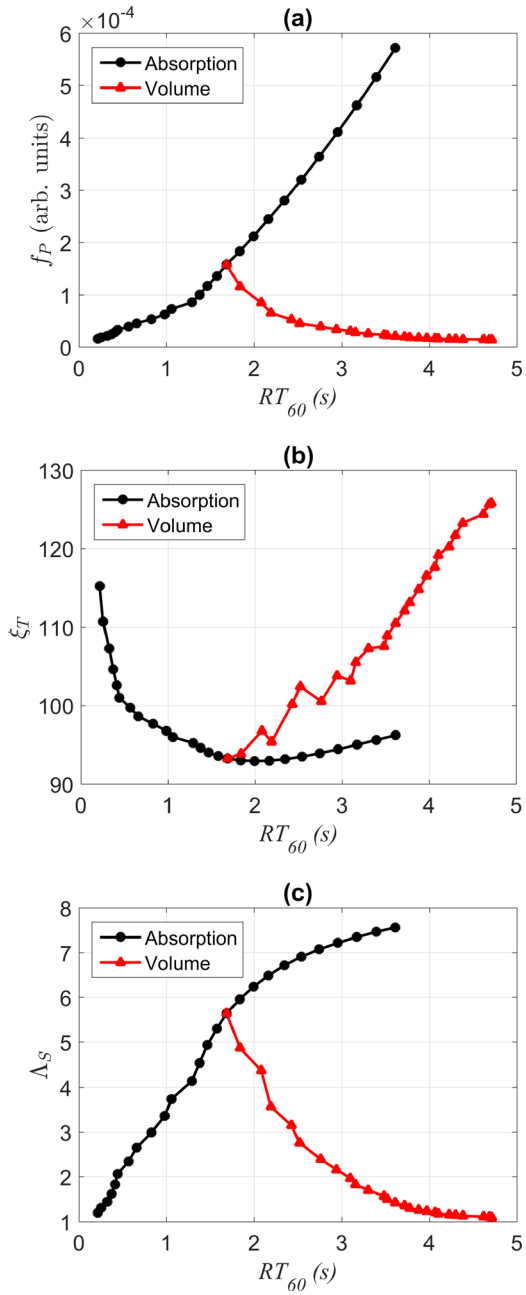

FIG. 7. (Color online) Simulation results for time reversal focusing metrics versus RT_{60} for various rooms of different frequency-dependent absorption coefficients and room volumes. (a) Peak focal amplitude, f_p. (b) Temporal quality, ξ_T. (c) Spatial clarity, Λ_s.

a G.R.A.S. 12AX constant current power module, was used to record the signals. A 14-bit Spectrum M2i.6022 generator was used to generate signals broadcast by the loudspeaker and a 16-bit Spectrum M2i.4931 digitizer was used to acquire the microphone signal with a 50 kHz sampling rate. During the first step of the TR process, a band-limited, 3 s duration, linear-chirp signal spanning from 500 to 7500 Hz is broadcast from the dodecahedron loudspeaker, and the microphone records the chirp response. The cross correlation between the chirp signal and the chirp response is used to approximate $h_{AB}(t)$ between the loudspeaker and microphone.[28] $h_{AB}(-t)$ is then calculated, normalized, and broadcast from the loudspeaker. The resulting signal at the microphone is the focal signal. The focal signal is then filtered between 500 and 7500 Hz with an eighth order, linear phase, bandpass infinite impulse response (IIR) filter to eliminate noise present outside of the excited frequencies. f_P and ξ_T are then calculated for each measurement. The spatial extent of the focusing is not measured in these experiments.

A. Changing absorption

A reverberation chamber with dimensions $4.96 \times 5.89 \times 6.98$ m (204 m^3) was used to test the effect that changing absorption has on TR. Twenty-four large foam anechoic wedges ($0.30 \times 0.30 \times 0.95$ m) were incrementally added to the floor of the reverberation chamber to lower the reverberation time from 8.1 s down to 1.5 s. However, this absorption could neither be applied uniformly throughout the room nor was the absorption applied uniformly on one surface within the room. The process outlined in the previous paragraph was followed using five averages for both measuring the impulse response and focal signal. f_P and ξ_T were determined for six different amounts of wedges (0, 2, 4, 8, 16, and 24). Reverse Schroeder integration[37,38] was used to determine each RT_{60} (8.1, 5.7, 4.5, 3.0, 1.8, and 1.5 s, respectively). Figure 8 shows a photograph of the experimental configuration with 24 wedges.

Image source simulations were created for each wedge configuration by increasing the absorption coefficient of only the floor surface (the absorption coefficients for the other five walls were held constant) by the appropriate amount to achieve each measured RT_{60}. Figure 9 compares simulated with measured f_P with respect to RT_{60}. In the simulations, the amplitudes were uniformly scaled to better match the experimental data trend. These results show the expected linear trend of f_P with increasing RT_{60} ($R^2 = 0.9940$), confirming the results shown in Fig. 5 pertaining to changing absorption and matching the assertion of Ribay *et al.*[16] The absolute values for ξ_T are greater for the simulated data than the measured data. This is likely due to the sensitivity of ξ_T to noise. According to Eq. (4), noise in experimental data increases the summation result in the denominator, leading to a lower value of ξ_T. This also leads to higher values of ξ_T for the noiseless simulations. The simulations of this room suggest there is no

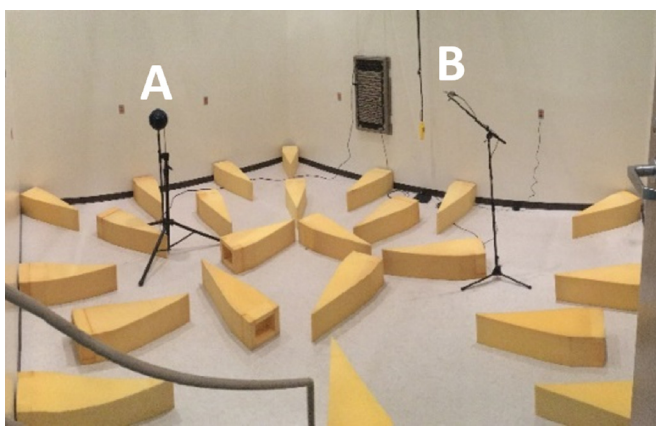

FIG. 8. (Color online) Photograph of the experimental set up in a reverberation chamber with 24 wedges. A is the location of the dodecahedron sound source and B is the location of the random-incidence microphone.

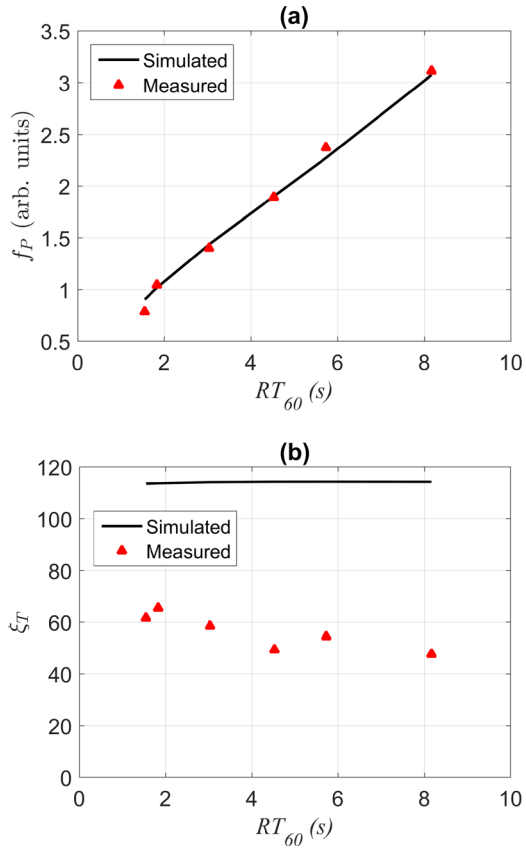

FIG. 9. (Color online) Experimental results obtained in the room shown in Fig. 8. (a) Peak focal amplitude, f_p, versus RT_{60} as a result of changing absorption. (b) Temporal quality, ξ_T, versus RT_{60} as a result of changing absorption with filtered focal signals.

dependence of ξ_T on RT_{60}, while the experimental results show a decreasing trend. The reason for this discrepancy is unknown but may be due to the uneven distribution of the foam wedges on the floor in the experimental case, whereas the simulated room had a uniform absorption coefficient for the floor.

B. Changing volume

Experimentally validating the effects that changing volume has on TR required multiple rooms with the same absorption characteristics (or at least similar absorption characteristics) but with different volumes. A multi-purpose room with two room dividers each having high transmission loss was chosen for its ability to easily change volume while maintaining similar absorption characteristics. With two room dividers, this multi-purpose room allowed for six different volume conditions: three small volume rooms with all room dividers closed, two medium volume rooms with one of the room dividers closed, and one large room with all room dividers open. This resulted in the following room volumes: 64, 73, 79, 137, 151, and 215 m^3, which resulted in RT_{60} values of 0.482, 0.485, 0.487, 0.498, 0.499, and 0.502 s, respectively, estimated using Eq. (6). Absorption coefficients in these rooms were assumed using the absorption coefficients of building materials found in standard tables.[39] Areas of absorbing surfaces and volumes were carefully determined by measurement. RT_{60} values obtained using reverse Schroeder integration applied to the measured impulse responses could not be done due to the very limited amount of decaying reverberation in these impulse responses. Additionally, the early reflections recorded in these responses do not smoothly decay, causing the values of RT_{60} to vary dramatically depending on the start and end times of the integration used (this is why the standard suggests avoiding the first 5 dB of decay in impulse responses). These rooms were simulated by computing average absorption coefficients for each individual wall surface since the Allen and Berkley code can only model each individual wall as having a uniform absorption.

Figure 10 shows an example of one of the medium room configurations with a volume of 137 m^3 with source and receiver locations identified. For each measurement, the dodecahedron loudspeaker and microphone were placed 3.0 m apart. Any changes in the direct sound between source and receiver have an effect on the TR process, thus a constant source to receiver distance is vital to isolating the effects that room volume has on TR. Two measurements were taken in each of the small volume rooms; one with the dodecahedron loudspeaker at the far end of the room and the microphone at the near end of the room (as seen in Fig. 10), and the other with the source and receiver positions interchanged. Six measurements were taken in the medium and large volume rooms: two with the midpoint between the loudspeaker and microphone near the center of the room and four with midpoints near the centers of each small volume room that comprises the medium or large volume rooms. Each pair of measurements followed the same loudspeaker and microphone location interchange that occurred in the small volume room measurements.

Figure 11 shows the results from the 24 different measurements. Although there is a notable variance in values of f_p for each RT_{60}, there is evidence that mean value of f_p for each room condition decreases with RT_{60} (statistical

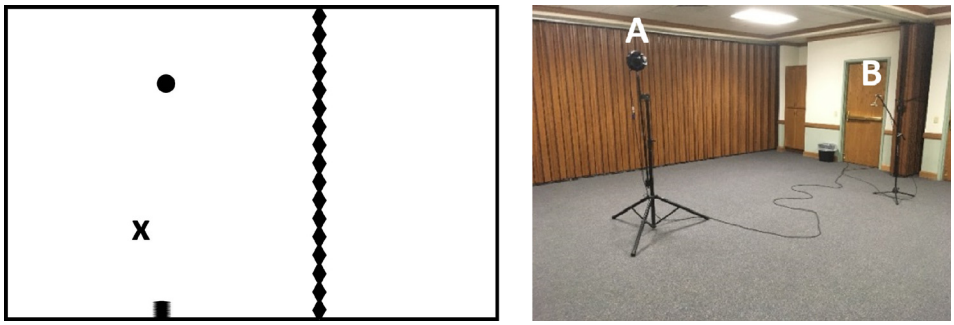

FIG. 10. (Color online) (left) Source A and receiver B locations in a medium room configuration with one room divider closed and the other open. (right) A photograph representing this same configuration where A is the location of the dodecahedron sound source and B is the location of the random-incidence microphone.

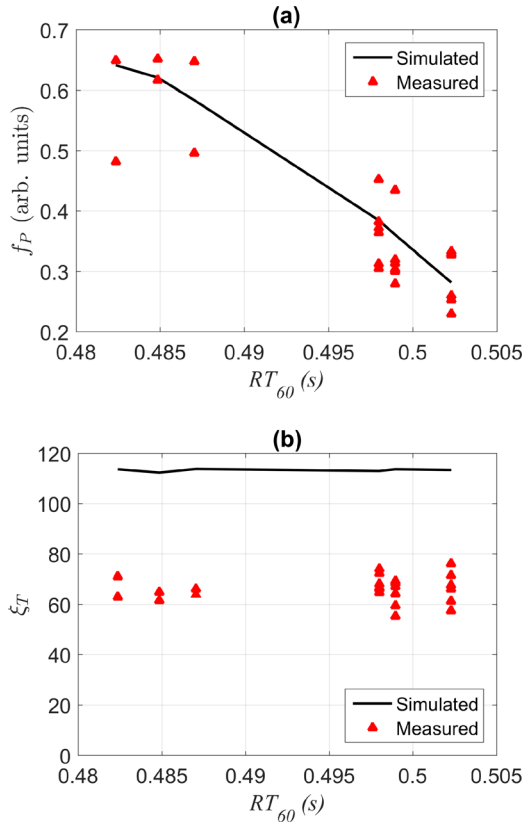

FIG. 11. (Color online) Experimental results obtained in the room shown in Fig. 10. (a) Peak focal amplitude, f_p, versus RT_{60} as a result of changing volume. (b) Temporal quality, ξ_T, versus RT_{60} as a result of changing absorption with filtered focal signals.

probability value <0.0001). This decreasing trend agrees with the simulation results for the changing volume case displayed in Fig. 5 and, thus, also disagrees with the assertion of Ribay *et al.*[16] The experimental and simulation results for ξ_T in Fig. 11 agree in that neither has a strong dependence on RT_{60}. From Fig. 5, it would be expected that ξ_T should increase with increasing RT_{60}. The apparent discrepancy between the simulation results in Figs. 5 and 11 may be due to the limited range of values in RT_{60} leading to a limited dataset for ξ_T or the fact that the absorption properties of the room used here did not stay perfectly constant when the volume was increased. The absolute values for ξ_T are greater for the simulated data than the measured data for the same reasons given in Sec. IV A.

V. CONCLUSION

The absorption characteristics and volume of a room have significant and differing impacts on TR focusing. Image source modeling has been used to determine the effects that changing absorption and volume have on peak focal amplitude, f_p, temporal quality, ξ_T, and spatial clarity, Λ_s. Less absorption increases f_p and Λ_s while decreasing ξ_T slightly. Dissimilarly, larger volumes decrease f_p and Λ_s while increasing ξ_T. The reasons can be traced back to the effect of absorption and volume on the reverberant field and proximity of image sources to the actual source. Higher absorption and larger volumes lead to lower-amplitude reflected arrivals. Higher amplitude reflected arrivals lead to improved f_p and Λ_s and diminished ξ_T, thus smaller, reverberant rooms with high-amplitude early arrivals produce the highest f_p and Λ_s. Another possible explanation of the different trend observed here when the room volume changes compared to the Ribay *et al.*[16] formula is that the underlying theory was developed for diffuse and ergodic cavities (this is also the case for the Quieffin theory[29,34]), whereas the rooms in this paper are diffuse but may not be considered ergodic, and the aforementioned works did not take into account direct arrivals. Limited experimental results confirmed expected trends for f_p. Experimental confirmation of the trends in ξ_T seen in simulated results were limited; further work should be conducted in a more ideal set of rooms.

The relationship between f_p and RT_{60} proposed by Ribay *et al.*[16] was confirmed only if RT_{60} is changed via changing absorption. The relationship is not true if RT_{60} is changed via changing volume. Larger volume rooms with similar absorption characteristics compared to smaller rooms result in lower values of f_p. For larger rooms, the early reflections arrive later in time and have undergone more spherical spreading loss than in smaller rooms and would thus contribute less to TR focusing.

Many TR applications that involve communication of signals require high ξ_T. This paper presents the first known analysis of the effects of room absorption and volume on ξ_T. A decrease in ξ_T indicates a distorted carrier signal for communications, thus it is important to understand what conditions lead to high values of ξ_T. Λ_s is defined for the first time. It is unique in relation to other metrics designed to measure spatial focusing in that it compares the value of ξ_T at the focus location to the values of ξ_T at other locations. This is useful for applications where strong temporal focusing is desired only at the focus location.

ACKNOWLEDGMENTS

Funding was provided by Brigham Young University's College of Physical and Mathematical Sciences and the Department of Physics and Astronomy.

[1]A. Parvulescu and C. S. Clay, "Reproducibility of signal transmission in the ocean," Radio Elec. Eng. **29**, 223–228 (1965).
[2]C. S. Clay and B. E. Anderson, "Matched signals: The beginnings of time reversal," Proc. Meet. Acoust. **12**, 055001 (2011).
[3]M. Fink, "Time reversed acoustics," Phys. Today **50**(3), 34–40 (1997).
[4]B. E. Anderson, M. Griffa, C. Larmat, T. J. Ulrich, and P. A. Johnson, "Time reversal," Acoust. Today **4**(1), 5–16 (2008).
[5]J.-L. Thomas, F. Wu, and M. Fink, "Time reversal focusing applied to lithotripsy," Ultrasonic Imag. **18**(2), 106–121 (1996).
[6]C. S. Larmat, R. A. Guyer, and P. A. Johnson, "Time-reversal methods in geophysics," Phys. Today **63**(8), 31–35 (2010).
[7]J. V. Candy, A. J. Poggio, D. H. Chambers, B. L. Guidry, C. L. Robbins, and C. A. Kent "Multichannel time-reversal processing for acoustic communications in a highly reverberant environment," J. Acoust. Soc. Am. **118**(4), 2339–2354 (2005).
[8]H. C. Song, "An overview of underwater time-reversal communication," IEEE J. Oceanic Eng. **41**(3), 644–655 (2016).
[9]L. P. Maia, A. Silva, and S. M. Jesus, "Environmental model-based time-reversal underwater communications," IEEE Access **6**, 10041–100051 (2018).
[10]B. E. Anderson, M. Griffa, T. J. Ulrich, P.-Y. Le Bas, R. A. Guyer, and P. A. Johnson, "Crack localization and characterization in solid media using time reversal techniques," in *Proceedings of the 44th U.S. Rock*

Mechanics Symposium and 5th U.S.-Canada Rock Mechanics Symposium, Salt Lake City, Utah (June 27–30, 2010), Paper No. 10-154.
[11]B. E. Anderson, L. Pieczonka, M. C. Remillieux, T. J. Ulrich, and P.-Y. Le Bas, "Stress corrosion crack depth investigation using the time reversed elastic nonlinearity diagnostic," J. Acoust. Soc. Am. **141**(1), EL76–EL81 (2017).
[12]M. Tanter, J. Thomas, and M. Fink, "Time reversal and the inverse filter," J. Acoust. Soc. Am. **108**(1), 223–234 (2000).
[13]J. V. Candy, A. W. Meyer, A. J. Poggio, and B. L. Guidry, "Time-reversal processing for an acoustic communications experiment in a highly reverberant environment," J. Acoust. Soc. Am. **115**(4), 1621–1631 (2004).
[14]A. W. Meyer, J. V. Candy, and A. J. Poggio, "Time reversal signal processing in communications—A feasibility study," Lawrence Livermore National Laboratory Library, Livermore, CA (2002).
[15]S. Yon, M. Tanter, and M. Fink, "Sound focusing in rooms: The time-reversal approach," J. Acoust. Soc. Am. **113**(3), 1533–1543 (2003).
[16]G. Ribay, J. de Rosny, and M. Fink, "Time reversal of noise sources in a reverberation room," J. Acoust. Soc. Am. **117**(5), 2866–28720 (2005).
[17]C. Draeger and M. Fink, "One-channel time-reversal in chaotic cavities: Theoretical limits," J. Acoust. Soc. Am. **105**(2), 611–617 (1999).
[18]A. Derode, A. Tourin, and M. Fink, "Limits of time reversal focusing through multiple scattering: Long range correlation," J. Acoust. Soc. Am. **107**(6), 2987–2998 (2000).
[19]C. Draeger, J.-C. Aime, and M. Fink, "One-channel time reversal in chaotic cavities: Experimental results," J. Acoust. Soc. Am. **105**(2), 618–625 (1999).
[20]B. E. Anderson, M. Clemens, and M. L. Willardson, "The effect of transducer directivity on time reversal focusing," J. Acoust. Soc. Am. **142**(1), EL95–EL101 (2017).
[21]M. L. Willardson, B. E. Anderson, S. M. Young, M. H. Denison, and B. D. Patchett, "Time reversal focusing of high amplitude sound in a reverberation chamber," J. Acoust. Soc. Am. **143**(2), 696–705 (2018).
[22]R. Bracewell, *The Fourier Transform and Its Applications*, 2nd ed. (McGraw-Hill, New York, 1978), p. 46.
[23]J. H. Rindel, "The use of computer modeling in room acoustics," J. Vibroeng. **3**(4), 41–72 (2000).
[24]J. Allen and D. A. Berkley, "Image method for efficiently simulating small-room acoustics," J. Acoust. Soc. Am. **65**(4), 943–950 (1979).
[25]P. M. Peterson, "Simulating the response of multiple microphones to a single acoustic source in a reverberant room," J. Acoust. Soc. Am. **80**(5), 1527–1529 (1986).
[26]E. A. Lehmann and A. M. Johansson, "Prediction of energy decay in room impulse responses simulated with an image-source model," J. Acoust. Soc. Am. **124**(1), 269–277 (2008).
[27]T. J. Ulrich, B. E. Anderson, P.-Y. Le Bas, C. Payan, J. Douma, and R. Snieder, "Improving time reversal focusing through deconvolution: 20 questions," Proc. Meet. Acoust. **16**, 045015 (2012).
[28]C. Heaton, B. E. Anderson, and S. M. Young, "Time reversal focusing of elastic waves in plates for an educational demonstration," J. Acoust. Soc. Am. **141**(2), 1084–1092 (2017).
[29]N. Quieffin, S. Catheline, R. K. Ing, and M. Fink, "2D pseudo-array using an ultrasonic one channel time-reversal mirror," in *Proceedings of the IEEE Ultrasonics Symposium*, Montreal, Canada (August 24–27, 2004), pp. 801–804.
[30]M. R. Schroeder and K. H. Kuttruff, "On frequency response curves in rooms. Comparison of experimental, theoretical, and Monte Carlo results for the average frequency spacing between maxima," J. Acoust. Soc. Am. **34**(1), 76–80 (1962).
[31]ISO 3741:2010: *Acoustics—Determination of Sound Power and Sound Energy Levels of Noise Sources Using Sound Pressure—Precision Methods for Reverberation Test Rooms* (International Organization for Standardization, Geneva, Switzerland, 2010).
[32]C. F. Eyring, "Reverberation time in 'dead rooms'," J. Acoust. Soc. Am. **1**, 217–241 (1930).
[33]R. F. Norris, C. F. Burgess, and C. A. Andree, "An instrumental method of reverberation measurement," J. Acoust. Soc. Am. **1**, 366–372 (1930).
[34]N. Quieffin, "Etude du rayonnement acoustique de structures solides: Vers un système d'imagerie haute résolution" ("Study of the acoustic radiation of solid structures: towards a high resolution imaging system"), Ph.D. thesis, Université Pierre et Marie Curie, Paris, France (2004).
[35]R. Weaver, "The unreasonable effectiveness of random matrix theory for the vibrations and acoustics of complex structures," in *New Directions in Linear Acoustics and Vibration*, edtibed by M. Wright, and R. Weaver (Cambridge University Press, Cambridge, UK, 2010), Chap. 3, pp. 42–58.
[36]O. Bou Matar, Y. Li, S. Delrue, and K. Van Den Abeele, "Optimization of chaotic cavity transducers to nonlinear elastic imaging," in *Proceedings of the 10th French Acoustic Congress*, Lyon, France (April 12–16, 2010), pp. 1–6.
[37]M. R. Shroeder, "New method of measuring reverberation time," J. Acoust. Soc. Am. **37**(3), 409–412 (1965).
[38]ISO 3382:1997(E): *Acoustics-Measurement of the Reverberation Time of Rooms with Reference to other Acoustical Parameters* (International Organization for Standardization, Geneva, Switzerland, 1997).
[39]D. Davis and C. Davis, *Sound System Engineering*, 2nd ed. (Howard W. Sams & Co., Indianapolis, IN, 1987), p. 159.